

## Accepted Manuscript

Title: Effects of Si/Al Ratio and Pt Loading on Pt/SAPO-11 Catalysts in Hydroconversion of Jatropha Oil

Author: Ning Chen Shaofeng Gong Hisakazu Shirai  
Toshitaka Watanabe Eika W. Qian



PII: S0926-860X(13)00364-5  
DOI: <http://dx.doi.org/doi:10.1016/j.apcata.2013.06.034>  
Reference: APCATA 14294

To appear in: *Applied Catalysis A: General*

Received date: 20-4-2013  
Revised date: 19-6-2013  
Accepted date: 22-6-2013

Please cite this article as: N. Chen, S. Gong, H. Shirai, T. Watanabe, E.W. Qian, Effects of Si/Al Ratio and Pt Loading on Pt/SAPO-11 Catalysts in Hydroconversion of Jatropha Oil, *Applied Catalysis A, General* (2013), <http://dx.doi.org/10.1016/j.apcata.2013.06.034>

This is a PDF file of an unedited manuscript that has been accepted for publication. As a service to our customers we are providing this early version of the manuscript. The manuscript will undergo copyediting, typesetting, and review of the resulting proof before it is published in its final form. Please note that during the production process errors may be discovered which could affect the content, and all legal disclaimers that apply to the journal pertain.

# Effects of Si/Al Ratio and Pt Loading on Pt/SAPO-11 Catalysts in Hydroconversion of Jatropha Oil

Ning Chen, Shaofeng Gong, Hisakazu Shirai, Toshitaka Watanabe, Eika W. Qian\*

Graduate School of Bio-Applications and Systems Engineering, Tokyo University of Agriculture and  
Technology, 2-24-16, Nakacho, Koganei, Tokyo 184, Japan

Tel/Fax: 0081-42-388-7410

E-mail: [whqian@cc.tuat.ac.jp](mailto:whqian@cc.tuat.ac.jp)

## Highlight

Hydroconversion of Jatropha oil into *iso*-paraffin was achieved in one catalytic step.

The medium acid sites in SAPO-11 increased with the increase of Si/Al ratio.

Hydrotreatment of Jatropha oil were performed at various LHSV and Si/Al.

The mechanism of hydroconversion of methyl oleate was investigated.

A reaction network for hydroconversion of Jatropha oil was suggested.

## Abstract

A series of Pt/SAPO-11 catalysts were prepared with various Si/Al ratios and Pt loadings and characterized by using BET, XRD, XRF, and CO pulse adsorption, as well as  $^{29}\text{Si}$  NMR and  $\text{NH}_3$ -TPD techniques. Their catalytic performances in hydroconversion of Jatropha oil were tested with a fixed-bed flow reactor system. The isomerization activity increased with the Si/Al ratio because there were more medium acidic sites on the SAPO-11 supports. Pt/SAPO-11 catalysts with a Si/Al ratio of 0.4 demonstrated high activity for both deoxygenation and isomerization among catalysts with the same Pt loading. The deoxygenation, isomerization and cracking activities strongly depended the on Pt loading. The best activity was observed for the sample with a 3 wt% Pt loading, which generated an 83 % yield of *iso*-C15-18 hydrocarbons under the LHSV of  $0.5 \text{ h}^{-1}$ . Based on the mechanistic study of hydroconversion of methyl oleate, a reaction network for the hydroconversion of Jatropha oil was suggested.

**Keywords:** SAPO-11, Si/Al ratio, Pt loading, Jatropha oil hydroconversion, Methyl oleate

## 1. Introduction

Because of the declining availability of petroleum resources, environmental pollution, and increased demand for fuels, the development of renewable bio-fuels has become increasingly important. Biodiesel is a liquid fuel with combustion properties similar to petroleum diesel, but it is essentially free of sulfur, making it a cleaner burning fuel than petroleum diesel [1]. Among the transformation technologies utilized to produce biodiesel, transesterification, catalytic cracking and hydroprocessing remain the most heavily researched. Currently, FAMES (Fatty Acid Methyl Esters), which are produced by transesterification, are frequently used as a component in diesel blends [2]. However, because FAMES have unsaturated bonds and approximately 10 wt% oxygen content, their blending volume is limited. Catalytic cracking, could achieve complete deoxygenation, yield low diesel fraction hydrocarbons and the formation of products with high olefin and aromatic compound content [3]. Consequently, hydroprocessing is importance for the development of technologies that facilitate for the utilization during the production of renewable bio-fuels [4,5].

The Hydrotreatment of vegetable oils content two principal reactions: hydrodeoxygenation and isomerization. Many researchers have investigated the hydrodeoxygenation of vegetable oils, such as palm oil [6], rapeseed oil [7-10], sunflower oil [11,12], and Jatropha oil [13,14], over conventional hydrotreatment catalysts, such as sulfided NiMo/Al<sub>2</sub>O<sub>3</sub>, CoMo/Al<sub>2</sub>O<sub>3</sub>, and NiW/Al<sub>2</sub>O<sub>3</sub>. Additionally, PtPd/Al<sub>2</sub>O<sub>3</sub> [15], CoMo/Carbon [16,17], and Pd/Carbon [18-20] have exhibited desirable deoxygenation activity to yield high amounts of hydrocarbons. However, these liquid hydrocarbon products consisted primarily of C<sub>15</sub> - C<sub>18</sub> *n*-alkanes. This group of alkanes demonstrates unfavorable cold flow properties (cloud point: 15-21 °C), which strictly limit their application.

The isomerization of *n*-paraffins is a feasible and promising method to improve cold flow properties in the petroleum industry [21,22]. The hydroisomerization of deoxygenated vegetable oils over Pt/Zeolite catalysts has been reported [23]. Although high-quality products (CFPP: -20 ~ -15 °C;

cetane number > 80) were obtained, cost of using a two-step process is quite high. Therefore, it is necessary to enact the conversion of vegetable oil into *iso*-paraffin in a single catalytic step.

The deoxygenation of vegetable oil to form *n*-alkanes and the subsequent isomerization of *n*-alkanes to form *iso*-alkanes are the two reactions necessary to hydroconvert vegetable oils into high-quality bio-fuels. Previous reports described bifunctional catalysts that loaded a noble metal (Pd or Pt) onto a 10-ring one-dimensional molecular sieve, such as SAPO-11 [24], ZSM-22 [25,26] or Theta-1 [27], performed the isomerization reaction competently. In particular, the Pt/SAPO-11 catalyst demonstrated a high isomerization/cracking ratio [28,29].

Although many reports describing the hydrotreatment of vegetable oil and model compounds have been disclosed, few of them described catalytic one-step process. We have previously reported a one-step process that utilized NiMo/SiO<sub>2</sub>-Al<sub>2</sub>O<sub>3</sub> and NiMo/SiO<sub>2</sub>-ZSM-5 catalysts [30], but the selectivity of the isomerization was insufficient to overcome the problematic cold flow properties. Additionally, 0.6 wt% Pt loaded on an acidic support might provide sufficient hydrogenation-dehydrogenation activity to match the acid sites [31]. However, some reports indicated that olefin hydrotreatment and deoxygenation reactions as well as some stepwise isomerization of *n*-paraffins, occur at the same active sites (metallic sites) [32]. Therefore, the competition of reactants might decrease the isomerization activity and cause the 0.6 wt% Pt loading to become insufficient.

Consequently, the aim of present work is to elucidate the details of the direct hydroconversion of vegetable oil during the generation of *iso*-paraffins over a Pt/SAPO-11 catalyst. Pt/SAPO-11 catalysts with different Pt contents and Si/Al ratios were prepared, and their catalytic performances in the hydroconversion of *Jatropha* oil were investigated. Furthermore, the hydroconversion of a model compound, methyl oleate, was also conducted to investigate the reaction mechanism.

## 2. Experimental

### 2.1. Materials

Crude *Jatropha* oil, which was produced in Bogor, Indonesia and supplied by CREATA-IPB, was used as the feedstock during the evaluation of catalytic activity. The composition of the feedstock directly affects the distribution of the hydrocarbon products, as well as catalytic activity. In addition to some physical properties, the chemical composition of the crude *Jatropha* oil was determined, and the results are presented in Table 1. The density and dynamic viscosity were determined with a hydrometer (JIS-II) and a dynamic viscometer (SV-10A; Vibro), respectively. The acid value, cloud point, and cetane index were determined according to ASTM-D974, ASTM-D5773, and ASTM-D4737, respectively. The fatty acid composition of the feedstock was determined by gas chromatography after transesterification and esterification with methanol. A CHNS/O elemental analyzer (2400II, PerkinElmer Japan) was used to determine the elemental composition of *Jatropha* oil. Additionally, a decalin (GR grade; Kishida Chemical Co. Ltd.) solution containing 1 wt% methyl oleate (>99 %; Aldrich Chemical Co. Inc.) was used to feed the model chemical experiments.

### 2.2. Catalyst preparation

The SAPO-11 samples were synthesized hydrothermally according to a previously reported procedure [33]. Aluminum isopropoxide, phosphoric acid and silica gel were used as Al, P, and Si sources, respectively. A mixture of di-*n*-propylamine and di-*iso*-propylamine with a mole ratio of 2:1 was used as the structure-directing agent. The molar compositions of the synthesis gels were 1.0 P: 1.0 Al:  $x$  Si: 0.75 R: 30 H<sub>2</sub>O ( $x = 0.1, 0.2, 0.4$  and  $0.8$ ), where R represents the template mixture. The SAPO-11 samples were washed, filtered, and calcined at 550 °C for 4 h in air to remove the template. These SAPO-11 samples were designated as SAPO-11(0.1), SAPO-11(0.2), SAPO-11(0.4), and SAPO-11(0.8).

The SAPO-11 supports were prepared according to the following procedure: first, 90 wt%SAPO-11, 10 wt% alumina sol, and a small amount of deionized water were stirred to produce a mud-like solid. Subsequently, the mud-like solid was pressed and shaped into small cylinders with an experimental scale model. Finally, the small cylinders were dried at room temperature for 12 h before being calcined in a muffle furnace at 550 °C for 3 h.

The above SAPO-11 samples were crushed and sieved to procure a 20–80 mesh particle size. Next, these SAPO-11 particles were impregnated with aqueous solutions of  $\text{H}_2\text{PtCl}_6$  to prepare the Pt/SAPO-11 catalysts in accordance with the conventional impregnation method procedures [34]. Catalysts A, B, and D were prepared, respectively with the SAPO-11(0.1), SAPO-11(0.2), and SAPO-11(0.8) supports to achieve a Pt loading of 0.6 wt%. Catalysts C, E, and F were prepared with the SAPO-11(0.4) support to achieve Pt loading amounts of 0.6 wt%, 1.5 wt%, and 3.0 wt%, respectively. After impregnation, the catalysts were dried at 105 °C for 2 h before being calcined at 450 °C for 4 h in air.

### 2.3 Characterization of catalysts

The XRD patterns were recorded with an X-ray diffractometer (RAD-IIC; Rigaku Corp.) with  $\text{Cu-K}\alpha$  radiation. The elemental analysis was conducted with an X-ray fluorescence instrument (EDX-800; Shimadzu Corp.). The samples were pressed into disks before analysis. The specific surface areas and pore sizes were determined from nitrogen adsorption and desorption isotherms recorded at  $-196$  °C (Belsorp-mini II; Bel Japan Inc.). Prior to be measured, the samples were degassed under vacuum at 400 °C for 1 h. The specific surface areas and pore volumes were calculated by using the Brunauer–Emmett–Teller (BET) method. The  $\text{NH}_3$ -TPD experiments were conducted with a chemisorption–physisorption analyzer (ChemBET PULSAR TPR/TPD; Quantachrome Instruments) according to the following procedure: first, approximately 200 mg of sample was loaded into the sample cell and pretreated under a 15 mL/min flow of hydrogen at 400 °C for 3 h. Subsequently, the sample was pretreated at 500 °C under a 15 mL/min flow of helium for 3 h. Furthermore, after cooling to 100 °C,

the ammonia adsorption was conducted for 40 min under ammonia flowing at 15 mL/min. The physically adsorbed ammonia was removed with a stream of helium at 100 °C for 2 h. Finally, the NH<sub>3</sub>-TPD of the samples was conducted by linearly increasing the cell temperature from 100 °C to 650 °C with a heating rate of 10 °C/min and a helium flow rate of 15 mL/min. The chemisorption of carbon monoxide was performed with the same equipment as the NH<sub>3</sub>-TPD at 30 °C to determine the dispersion of active metals. The chemisorption stoichiometry considered to calculate the number of active sites was 1:1. Solid-state <sup>29</sup>Si NMR experiments were conducted on a JEOL JNM-ECX 400 spectrometer with a resonance frequency of 78.65 MHz. The <sup>29</sup>Si MAS spectra were recorded at a pulse width of 4 μs, a recycle delay of 60 s, and a rotor-spinning rate of 7 KHz. Tetramethyl silane (TMS) was used as an external standard.

#### 2.4 Test of catalyst activity

The details of our experimental apparatus were presented in an earlier report [35]. Briefly, the reactions were conducted in a fixed-bed flow microreactor (8 mm i.d.). Approximately 3 mL of catalyst was diluted with SiC and loaded in the reactor. The feedstock was injected into the hydrogen stream with a high-pressure pump. The reaction of Jatropha oil was conducted at 350 °C, 3 MPa total pressure, with liquid hourly space velocity (LHSV) of 0.25-2 h<sup>-1</sup>, and a H<sub>2</sub>/feed ratio of 1200 (v/v). The reaction of methyl oleate was conducted at 200–325 °C, 3 MPa of total pressure, with a liquid hourly space velocity (LHSV) of 40 h<sup>-1</sup>, and a H<sub>2</sub>/feed ratio of 1200 (v/v). Before reaction, all catalysts were reduced *in situ* at 400 °C for 3 h under an atmosphere of a H<sub>2</sub> flow at a rate of 50 mL/min. The catalytic activity was measured after stabilization (total time on stream was approximate 10 h).

After reaction, the gaseous and liquid products were separated. Two gas chromatographs (GC-2025 and GC-14B; Shimadzu Corp.), which were each equipped with a flame ionization detector (FID) and a commercially available column (DB-1, 0.25 mm × 60 m), were used to analyze the hydrocarbons in the gaseous and liquid products. A CP-TAP CB for triglycerides column (0.25 mm × 25 m) was used to

analyze the heavy products, such as monoglycerides, diglycerides, and triglycerides. Additionally, a gas chromatograph mass spectrometer (GCMS-QP5050A; Shimadzu Corp.) equipped with the same capillary column as above (DB-1, 0.25 mm × 60 m) was used to analyze the hydrocarbon products. Another gas chromatograph (GC-8A; Shimadzu Corp.), which had a thermal conductivity detector (TCD) and a commercial column (Unibeads C, 3 mm × 3 m), was used to determine other components, such as CO and CO<sub>2</sub>, in the gaseous products.

The product mixtures obtained from hydroconversion of Jatropha oil were separated into gaseous, water and oil phases. The gaseous products consisted of a large amount of propane from hydrogenation of glycerin and small amounts of other light hydrocarbons (C<sub>1-4</sub>) that resulted from cracking and methanation reactions. Carbon dioxide and carbon monoxide, which were generated from decarbonylation/decarboxylation pathways, were also detected. The oil phase consisted of hydrocarbons (C<sub>5-18+</sub>), as well as trace amounts of free fatty acid (stearic acid and palmitic acid), fatty alcohol (octadecanol, heptadecanol, hexadecanol, pentadecanol) and esters (stearyl stearate). In addition monoglycerides, diglycerides and unreacted triglycerides were also detected in the oil phase.

The individual products were identified through GC standards. The conversion of triglycerides in Jatropha oil was calculated as:

$$C (\%) = 100\% - C_{TG}$$

where  $C_{TG}$  is the concentration of triglyceride in the product oil. The deoxygenation rate was calculated as follows:

$$HDO (\%) = (\sum_{\text{feedstock}} - \sum_{\text{product}}) / \sum_{\text{feedstock}} \times 100$$

where  $\sum_{\text{feedstock}}$  and  $\sum_{\text{product}}$  indicate the molar amount of total oxygen in the feedstock and products, respectively.

### 3. Results and discussion

#### 3.1. Characterization of supports and catalysts.

Fig. 1 shows the powder XRD patterns of four SAPO-11 samples. An AEL structure (i.e.,  $2\theta = 8.1^\circ$ ,  $9.4^\circ$ ,  $13.1^\circ$ ,  $15.6^\circ$ ,  $20.3^\circ$ ,  $21.0^\circ$ ,  $22.1^\circ$ - $23.2^\circ$ ) was obtained for all samples [36]. However, when the Si/Al ratio increased, the crystallinity decreased gradually (Table 2). In particular, SAPO-11(0.8) suffered a 42% decrease in crystallinity, in which a certain amount of amorphous alumina-phosphorous phase was formed. The BET surface area and microporous volume of the samples are presented in Table 2. The BET surface area and microporous volume of samples also decreased with the increased Si/Al ratio. SAPO-11(0.8) had a surface area of  $129 \text{ m}^2/\text{g}$ , which was much smaller than observed for other samples because the excessive silicon caused the decrease in crystallinity. These results demonstrate that an exorbitant increase in the Si/Al ratio in the synthesis system will destroy the crystal structure of SAPO-11.

The surface acid properties of the SAPO-11 samples were investigated via  $\text{NH}_3$ -TPD and the results are displayed in Fig. 2. All SAPO-11 samples exhibited a similar distribution of acidic sites. The profiles contained two  $\text{NH}_3$  desorption peaks: a sharp peak at ca.  $250^\circ\text{C}$  and a shoulder peak at ca.  $345^\circ\text{C}$ , corresponding the weak and medium acid sites, respectively. To compare the distribution of acidity between these samples, the  $\text{NH}_3$ -TPD profiles were separated into two peaks by fitting the curves with a Gaussian function [29,30]; the amount of each type of acid site was calculated and presented in Table 3. It could be observed that the amount of medium acidic sites increased with an increase in the Si content; however, the number of weak and total acidic sites did not display this relationship. SAPO-11(0.2) had largest number of weak acidic sites, whereas SAPO-11(0.4) had the most total acidic sites. These results indicated that the acidity of SAPO-11 samples did not have a positive linear relationship with the silicon content, which was most likely because the Si incorporation mechanism in the framework was different across SAPO-11 samples with varying Si contents.

Aluminophosphate molecular sieves ( $\text{AlPO}_4\text{-n}$ ) are composed strictly alternating  $\text{AlO}_4$  and  $\text{PO}_4$  tetrahedral structures and have a neutral framework without extra framework cations. The incorporation of Si produces silicoaluminophosphate molecular sieves (SAPO-n), which develop negative charges on

the aluminophosphate framework. Consequently, Brønsted acidity or ion-exchange capacity results [37]. However, unlike aluminosilicate zeolites, the number of Brønsted acid sites in SAPO-*n* depends not only on the chemical composition of the SAPO materials, but also on the mode of Si incorporation into the framework [38]. The incorporation of Si atoms into aluminophosphate frameworks occurs through two mechanisms (SM2 and SM3) [39]. One mechanism is the substitution of a Si atom for a P atom (SM2), which will generate a Si atom with four neighboring Al atoms and give rise to weak acid sites. The second mechanism is the substitution of two Si atoms for a pair of Al and P atoms (SM3). Concurrently, the substitution of three Si atoms for three P atoms adjacent to a substituted Al atom occurs to avoid the formation of Si–O–P linkages. This substitution engenders the formation of silica islands composed of at least five Si atoms. In this case, in the edge of these silica islands, Si–O–Al linkages will generate acid sites similar to aluminosilicate zeolites. The acid sites that originated from these Al atoms are more acidic than the sites formed by SM2.

<sup>29</sup>Si MAS NMR experiments were performed to investigate the local environments of the Si atoms in SAPO-11 samples with varying Si incorporation, and the results are presented in Fig. 3. There are marked differences in the Si distribution between these samples. To illustrate the presence of different Si environments, the NMR spectra were converted into five simulated peaks by fitting the curves with a Gaussian function. The five peaks centered at ca. –112, –107, –102, –97, and –90 ppm can be attributed to Si(4Si), Si(1Al, 3Si), Si(2Al, 2Si), Si(3Al, Si) and Si(4Al) environments, respectively. The ratios of the various types of Si are listed in Table 4. According to the previously described Si incorporation mechanism [37], the SM2 mechanism only generates a Si(4Al) environment, but the SM3 mechanism forms Si(4Si), Si(1Al, 3Si), Si(2Al, 2Si), and Si(3Al, Si) environment. In addition, the proportion of Si(4Al) sites decreased but the ratio of the total Si(*n*Al, 4–*n*Si) sites with  $4 > n > 0$  increased when the Si content increased. These results indicated that the SM3 substitution mechanism increased with the Si content of the SAPO-11 samples, but the SM2 substitution mechanism decreased under the same

condition. The results also demonstrate that the amount of Si(4Si) environment increased continuously with the Si content, which might be ascribed to the formation of large silica islands.

The physicochemical properties of the calcined catalysts are presented in Table 5. When loaded with an active metal, all of the catalysts undergo a decrease in specific surface area. Catalyst D exhibited a much lower specific surface area than other catalysts because the SAPO-11(0.8) sample has a low specific surface area. Catalysts A, B, C, and D had a similar Pt loading, which varied from 0.55 to 0.58 wt%, whereas catalyst E and F had Pt loadings of 1.41 wt% and 2.78 wt%, respectively. Furthermore, the carbon monoxide chemisorption experiments demonstrated that the dispersion of Pt in the catalysts varied from 36 to 61%. Compared to catalysts A, B and C, catalyst D exhibited a marked reduction in Pt dispersion, even though all of these catalysts had a similar Pt loading. These results indicated that the amorphous alumina-phosphorous phase that appeared in SAPO-11(0.8) strongly affected the metal dispersion. In addition, the Pt dispersion decreased with the Pt loading, which is partly caused by the aggregation of the metal atoms.

### *3.2. Effects of the Si/Al Ratio on Hydroconversion of Jatropha Oil.*

It has been reported that 0.6 wt% Pt loaded onto an acidic support could provide sufficient hydrogenation-dehydrogenation function to match the acid sites [31]. Therefore, 0.6 wt% Pt was loaded onto the above SAPO-11 samples; the hydroconversion of Jatropha oil over various Pt/SAPO-11 catalysts (Catalysts A, B, C, and D) was conducted under the following conditions to investigate the Si/Al ratio: 350 °C, 3 MPa, volumetric H<sub>2</sub>/Oil ratio of 1200 and a liquid hourly space velocity (LHSV) of 1 h<sup>-1</sup>. The conversion of triglycerides in Jatropha oil and yield of various products over Catalysts A, B, C, and D are listed in Table 6. The triglycerides were almost completely converted by all of the catalysts (>98.3 %). In addition, a high yield (82.8–84.9 wt%) of liquid hydrocarbon products was achieved for all catalysts, whereas the yield of gaseous hydrocarbon and water varied from 5.6 wt% to 5.9 wt% and 7.5 wt% to 8.3 wt%, respectively. Catalyst D demonstrated a lower triglyceride conversion and water

yield than the other catalysts because its low specific surface area and Pt dispersion resulted in low hydrodeoxygenation activity.

The liquid hydrocarbon products were further divided into three groups: deoxygenated products ( $C_{15-18}$ ), cracking products ( $C_{5-14}$ ), and heavy products ( $C_{18+}$ ). As observed in Fig. 4, the  $C_{15-18}$  fraction was the major product of the deoxygenation of the free fatty acid groups in Jatropha oil, while the fraction  $C_{5-14}$  was produced by the cracking of the  $C_{15-18}$  products. Furthermore, the fraction  $C_{18+}$  contained mainly heavy alkanes derived from the polymerization, which occurred simultaneously with the cracking reaction, and a small amount of oxygenated products, such as fatty acids and fatty alcohols, from the incomplete deoxygenation of triglycerides. Compared to Catalyst A, B and C, the highest level of oxygenated compounds were found in fraction  $C_{18+}$  over Catalyst D because Catalyst D had a low Pt dispersion, which led to a low number of active Pt sites on SAPO-11. As well known that deoxygenation depends on metallic sites, and catalysts with a low number of active Pt sites will exhibit a lower conversion of triglycerides. In addition, the  $C_{15-18}$  fraction had a yield above 60 % over all of the catalysts. The yield of  $C_{5-14}$  fraction increased slightly with an increased Si/Al ratio, indicating that the present of more medium acidic sites (Table 3) enhanced the cracking activity.

Fig. 5 displays the yield of *iso*- $C_{15-18}$  hydrocarbon products versus the Si/Al ratio. The yield increased when the Si/Al ratio increased. In addition, the yield improved almost twofold when the Si/Al ratio rose from 0.1 to 0.2 or 0.2 to 0.4, although there was not as large of difference in isomerization between the ratios of 0.4 and 0.8. Taking account the  $NH_3$ -TPD result, it is suggested that the isomerization activity largely depended on the acidity of the supports. This result indicated that in Pt/SAPO-11 catalyst, Pt provided a strong metallic function whereas SAPO-11 had not enough acidity; the corresponding catalysts exhibited relatively weak acid function. For this reason, the skeletal isomerization was regarded as the rate-limiting step in isomerization. Therefore, it could be reasonably inferred that increasing the acidity of SAPO-11, which might be achieved by compositing it with more acidic support (e.g., ZSM-5 [40] or  $H\beta$  [41]), might enhance the isomerization activity.

### 3.3. Effects of Pt Loading and LHSV on Hydroconversion of Jatropha Oil.

Hydroconversion of Jatropha oil over SAPO-11 catalysts with different Pt loadings (Catalysts C, E, and F) was conducted under the following conditions: 350 °C, 3 MPa, a volumetric H<sub>2</sub>/Oil ratio of 1200 and varied liquid hourly space velocities (LHSV) of 0.25-2 h<sup>-1</sup>. Table 7 lists the conversions of triglycerides and the yields of various products. GC analysis proved that the C<sub>15-18</sub> hydrocarbons were the predominant reaction products of hydroconversion of Jatropha oil. No triglycerides were detected in the liquid products of any of the catalysts, indicating that all three catalysts had a good HDO performance. The yields of liquid hydrocarbons, gaseous hydrocarbons and water products were 65.3–83.2 wt%, 5.6–13.3 wt%, and 9.5–10.4 wt%, respectively. Additionally, with the increase in LHSV, the yield of liquid hydrocarbons increased, whereas the yield of gaseous hydrocarbons decreased. This is because increasing the LHSV would decrease the contact time, and the cracking reaction was suppressed. However, higher Pt loading generated decreased yields of liquid hydrocarbons and increased yields of gaseous hydrocarbons. These results indicate that the cracking activity of Pt/SAPO-11 catalyst increased concomitantly with higher Pt loading. For CO and CO<sub>2</sub>, the yield decreased markedly when the LHSV increased, whereas the yield of water changed only slightly. These results indicated that the LHSV did not strongly affect the deoxygenation pathway (hydrodeoxygenation, decarboxylation/decarbonylation), but instead influenced the methanation reaction.

The yields of various fractions are portrayed in Fig.6. When the LHSV increased, the yield of the C<sub>15-18</sub> and C<sub>18+</sub> fraction increased, whereas the yield of the C<sub>5-14</sub> fraction and the ratio of *iso*-C<sub>15-18</sub>/*n*-C<sub>15-18</sub> decreased. These results also indicated that the increase in LHSV decreased the contact time, which suppressed deoxygenation, isomerization, and cracking reactions. Fig. 7 presents the ratio of *iso*-C<sub>15-18</sub>/*n*-C<sub>15-18</sub> versus LHSV over Pt/SAPO-11 catalysts with varied Pt loading. When comparing various Pt loading, it was observed that with higher Pt loading, the yield of the C<sub>15-18</sub> and the C<sub>18+</sub> fraction

decreased, whereas the yield of  $C_{5-14}$  fraction and ratio of *iso*- $C_{15-18}/n$ - $C_{15-18}$  increased. The cracking, isomerization, and deoxygenation reactions in hydroconversion of Jatropha oil over Pt/SAPO-11 catalysts increased with the Pt loading. Corma et al. [42] investigated different metal loadings for Pt/MSA catalysts for hydroconversion of *n*-decane. Their results indicated that 0.6 wt% Pt loading on MSA with created the optimal balance between the acidic and metallic sites. In addition, when the Pt loading was lower or higher than 0.6 wt%, the isomerization was decreased due to the insufficient metallic activity or cracking, respectively. For the hydroconversion of Jatropha oil, however, the isomerization increased with Pt loadings from 0.6 to 3 wt%. It is suggested that the deoxygenation reaction and some step isomerization of *n*-paraffins might occur at the same active sites (Pt atoms). Therefore, the competition of the reactants for active sites had occurred and 0.6 wt% Pt loading was not sufficient to enact deoxygenation and isomerization simultaneously.

In addition, although Pt dispersion decreased with higher Pt loading (Table 5), the total number of Pt sites still increased. Therefore, the heightened deoxygenation was attributed to the larger number of Pt sites. Interestingly, the ratio of *iso*- $C_{15-18}/n$ - $C_{15-18}$  was extremely low with Catalyst C, but it increased considerably along with the Pt loading. Reportedly, the Pt/SAPO-11 catalyst, which has a Pt loading lower than 0.6 wt%, demonstrated relatively high activity in the isomerization of *n*-alkanes [43]. As mentioned above, the competition between the reactants might hinder the isomerization reactions. To verify the competition effect of the feedstock, the hydroisomerization of deoxygenated Jatropha oil, which was mostly comprised of *n*-paraffins (i.e., *n*- $C_{4-14}$ , 1.19 %; *n*- $C_{15-18}$ , 95.21 %; *iso*- $C_{4-18}$ , 2.54 %;  $C_{18+}$ , 1.06 %) was also studied over Catalyst C under the following conditions: 350 °C, 3 MPa and a LHSV of 2 h<sup>-1</sup> [29]. A much higher ratio of *iso*- $C_{15-18}/n$ - $C_{15-18}$  (15.1) in the liquid hydrocarbon products was obtained from the isomerization of the HDO-Oil than from the hydroconversion of Jatropha oil. Therefore, the feed had a dramatic effect on the isomerization activity of the Pt/SAPO-11 catalyst. The significant difference was most likely attributed to the limit diffusion of the reactant over the catalysts. The critical diameter of the triglyceride molecule was approximate 2 nm [44,45], whereas the SAPO-11

had only medium pores that were approximate  $0.65 \text{ nm} \times 0.4 \text{ nm}$  [46], which were much smaller than the triglyceride molecule. Therefore, the triglyceride molecules could not diffuse through the ordered micropores of the SAPO-11 catalysts, precluding efficient contact between the triglyceride molecules and the active sites; reactions could only occur on the external surface of the SAPO-11 catalysts. The critical diameters of *n*-alkanes nearly equaled  $0.43\text{--}0.49 \text{ nm}$  [21], which was smaller than the SAPO-11 micropores. Therefore, the *n*-alkanes could readily diffuse into the micropores of SAPO-11, and isomerization of *n*-alkanes proceeded on both the internal and external surfaces of the SAPO-11 catalysts. Because of the diffusion-limiting, the triglyceride molecules in *Jatropha* oil or oxygenated intermediates generated from hydrogenation of *Jatropha* oil were too large to diffuse into the ordered micropores of Pt/SAPO-11 catalyst. These oxygenated species must be deoxygenated into *n*-alkanes before entering the ordered micropores of Pt/SAPO-11 catalyst to generate *iso*-alkanes. Therefore, the deoxygenation activity of Pt/SAPO-11 catalyst was enhanced significantly by raising the Pt loading, which also facilitated the isomerization reactions. In addition, cracking and isomerization occurred simultaneously, but selectivity for the cracking product  $\text{C}_{5-14}$  increased with Pt loading. However, the excessively high Pt loading is not compatible with industrial applications. Using some non-noble metals in place of a portion of Pt might promote the deoxygenation and isomerization of vegetable oils at a reduced cost.

#### 3.4. Hydroconversion of Methyl Oleate.

To elucidate the reaction mechanism of hydroconversion of *Jatropha* oil, a model study with methyl oleate over Catalyst C was conducted under the following conditions:  $200\text{--}325 \text{ }^\circ\text{C}$ ,  $\text{LHSV} = 40 \text{ h}^{-1}$ ,  $3 \text{ MPa}$ , and  $\text{H}_2/\text{Oil} = 1200 \text{ ml/ml}$ . The detailed product distributions of methyl oleate hydroconversion are presented in Table 8.

Methyl oleate was almost completely converted, even at the relatively low temperature of  $200 \text{ }^\circ\text{C}$ . Oxygenated compounds were the main products at temperatures below  $275 \text{ }^\circ\text{C}$ , while the deoxygenation

rate was higher than 90 % at temperatures above 275 °C. Hydrocarbons with carbon number of 17 and 18 ( $C_{17-18}$ ) were the main products, and were regarded as products of hydrodeoxygenation, as well as decarbonylation or decarboxylation, respectively. The  $C_{17}/C_{18}$  ratios at various reaction temperatures were similarly close to 1.15, which indicated that the reaction temperature did not strongly affect the reaction pathway. The ratio of *iso*- $C_{17+18}/n$ - $C_{17+18}$  increased along with the reaction temperature because high temperatures might activate the acidic function of Pt/SAPO-11 catalyst to enhance the isomerization activity. All of the oxygenated compounds had straight chains, indicating that they were deoxygenated to form *n*-alkanes before isomerization.

The yields of various oxygenated compounds generated over catalyst C were plotted against the reaction temperature in Fig. 8. A high concentration of methyl stearate and small amount of other oxygenate intermediate products (i.e., octadecanol, stearic acid, heptadecanol, and octadecyl stearate) was generated at 200 °C. At higher temperatures, the concentration of methyl stearate decreased continuously, whereas the concentration of the other oxygenated intermediate products first increased and then decreased. Based on these results, we propose a reaction network for hydroconversion of methyl oleate over Pt/SAPO-11 catalyst. As shown in Scheme 1, in the first step, the unsaturated methyl oleate is hydrogenated quickly to form a saturated methyl stearate. In the second step, hydrogenolysis of methyl stearate occurs at the Pt active sites to generate stearic acid. Subsequently, stearic acid undergoes deoxygenated via three pathways: hydrodeoxygenation, decarbonylation and decarboxylation. In the hydrodeoxygenation route, octadecanol is formed by hydrogenolysis of stearic acid before being hydrogenated to produce octadecane. In the decarbonylation route, heptadecanol is formed through the decarbonylation of stearic acid before being hydrogenated to furnish heptadecane. Even with no direct evidence, previous studies agree that stearic acid can be transformed directly into heptadecane, which is formed via the decarboxylation route. Finally, octadecane and heptadecane isomerize to yield their branched isomers.

Water gas shift and methanation reactions were regarded as side-reactions during the hydrotreatment process and were the reason that the hydrogen consumption increased. Fig. 9 showed the experimental and theoretical yields of the gaseous products. Obviously, CO and CO<sub>2</sub> were almost entirely converted to CH<sub>4</sub>. These results indicated that the water gas shift and methanation reactions (as shown in Equations (1)-(3)) occurred with CO and CO<sub>2</sub> to generate methane.



Both methyl oleate and triglycerides in *Jatropha* oil are fatty acid esters. The reaction network for hydroconversion of *Jatropha* oil is similar to that of methyl oleate. According to the previous results, a reaction pathway has been proposed for hydroconversion of *Jatropha* oil over Pt/SAPO-11 catalyst (Scheme 2). In the first step of this reaction pathway, the triglyceride is hydrogenated to form a saturated triglyceride. Next, the saturated triglyceride is most likely broken down into diglyceride, monoglyceride, and other fatty acids through continuous hydrogenation. At the same time, the glycerol generates propane. Subsequently, the fatty acids are converted into *n*-alkanes via three different pathways: decarboxylation, decarbonylation and hydrodeoxygenation. Finally, the straight chain alkanes are transformed into their branched isomers.

#### 4. Conclusions

Four SAPO-11 samples were synthesized with different Si/Al ratios. The results indicated that the AEL structure was obtained in all SAPO-11 samples, but the crystallinity decreased when the Si/Al ratio increased. With greater incorporation of Si, the number of medium acidic sites increased, resulting in an enhanced isomerization activity. The <sup>29</sup>Si NMR results indicated that the SM3 substitution mechanism

increased, whereas the SM2 substitution mechanism decreased concomitantly with a larger Si/Al ratio; additionally, large silica islands were formed in SAPO-11 samples with high Si content.

The hydroconversion of Jatropha oil demonstrated that Pt/SAPO-11 catalyst could be a competent catalytic system for the single step hydroconversion of vegetable oil to biodiesel with a high content of *iso*-paraffins. The complete conversion of triglycerides was achieved over SAPO-11 (0.4) with different Pt loadings, and the highest ratio of *iso*-C<sub>15-18</sub>/*n*-C<sub>15-18</sub> was approached 22 with 3 wt% Pt/SAPO-11 under the condition of 350 °C and a LHSV of 0.5 h<sup>-1</sup>. Deoxygenation, isomerization and cracking reactions were strongly dependent on Pt loading due to its hydrogenation-dehydrogenation function. A mechanistic study of a model compound, methyl oleate, was carried out over catalyst C at varied temperatures. Methyl stearate, octadecanol, stearic acid, heptadecanol, and octadecyl stearate were determined to be components of the product mixture and regarded as intermediates of the hydrodeoxygenation of methyl oleate. Based on these results, a reaction network for hydroconversion of Jatropha oil was suggested. Triglycerides were first transformed into oxygenated intermediate molecules, and these oxygenates were then deoxygenated to form *n*-alkanes. Subsequently, the *n*-alkanes diffused into the ordered micropores of SAPO-11 for isomerization or cracking. Additionally, the deoxygenation of oxygenates to form *n*-alkanes was the rate-determining step in hydroconversion of triglycerides to *iso*-alkanes. Therefore, when the Pt loading was increased, the isomerization and cracking activities of Pt/SAPO-11 catalyst were enhanced significantly.

**References**

- [1] D.G. Cantrell, L.J. Gillie, A.F. Lee, K. Wilson, *Appl. Catal. A*. 287 (2005) 183-190.
- [2] G. Ramya, R. Sudhakar, J. Amala Infant Joice, R. Ramakrishnan, T. Sivakumar, *Appl. Catal. A*. 433 (2012) 170-178.
- [3] Z. Helwani, M.R. Othman, N. Aziz, J. Kim, W.J.N. Fernando, *Appl. Catal. A*. 363 (2009) 1-10.
- [4] T. Marker, J. Petri, T. Kalnes, M. McCall, D. Mackowiak, B. Jerosky, B. Reagan, L. Nemeth, M. Krawczyk, S. Czernik, D. Elliott, D. Shonnard, *Opportunities for Biorenewables in Oil Refineries, Final Technical Report of U.S. Department of Energy 2005.*
- [5] T. V. Choudhary, C. B. Phillips, *Appl. Catal. A*. 397 (2011) 1-12.
- [6] A. Guzman, J. E. Torres, L. P. Prada, M. L. Nuñez, *Catal. Today*. 156 (2010) 38-43.
- [7] I. Sebos, A. Matsoukas, V. Apostolopoulos, N. Papayannakos, *Fuel*. 88 (2009) 145-149.
- [8] P. Šimáček, D. Kubička, G. Šebor, M. Pospíšil, *Fuel*. 89 (2010) 611-615.
- [9] D. Kubička, L. Kalua, *Appl. Catal. A*. 372 (2010) 199-208.
- [10] R. Sotelo-Boyás, Y. Liu, T. Minowa, *Ind. Eng. Chem. Res.* 50 (2011) 2791-2799.
- [11] G. W. Huber, P. O'Connor, A. Corma, *Appl. Catal. A*. 329 (2007) 120-129.
- [12] D. Kubička, M. Bejblová, J. Vlk, *Top. Catal.* 53 (2010) 168-178.
- [13] Y. Liu, R. Sotelo-Boyás, K. Murata, T. Minowa, K. Sakanishi, *Chem. Lett.* 38 (2009) 552-553.
- [14] K. Murata, Y. Liu, M. Inaba, I. Takahara, *Energy Fuels*. 24 (2010) 2404-2409.
- [15] S. Gong, A. Shinozaki, M. Shi, E. W. Qian, *Energy Fuels*. 26 (2012) 2394-2399.
- [16] A. Centeno, E. Laurent, B. Delmon, *J. Catal.* 154 (1995) 288-298.
- [17] M. Ferrari, R. Maggi, B. Delmon, P. Grange, *J. Catal.* 198 (2001) 47-55.
- [18] M. Snåre, I. Kubičková, P. Mäki-Arvela, D. Chichova, K. Eränen, D. Y. Murzin, *Fuel*. 87 (2008) 933-945.
- [19] P. Mäki-Arvela, M. Snåre, K. Eränen, J. Myllyoja, D. Y. Murzin, *Fuel*. 87 (2008) 3543-3549.

- [20] I. Kubičková, M. Snáre, K. Eränen, P. Mäki-Arvela, D. Y. Murzin, *Catalysis Today*. 106 (2005) 197–200.
- [21] V. M. Akhmedov, S. H. Al-Khowaiter, *Catal. Rev.* 49 (2007) 33–139.
- [22] J. Hancsók, M. Krár, Sz. Magyar, L. Boda, A. Holló, D. Kalló, *Micro. Meso. Mater.* 101 (2007) 148–152.
- [23] R. Tiwari, B. S. Rana, R. Kumar, D. Verma, R. Kumar, R. K. Joshi, M. O. Garg, A. K. Sinha, *Catal. Commu.* 12 (2011) 559–562.
- [24] S. Miller, *J. Microporous Mater.* 2 (1994) 439–449.
- [25] F. G. Dwyer, E. W. Valyocsik, US Patent. 5336478, 1994.
- [26] M. C. Claude, G. Vanbutsele, J. A. Martens, *J. Catal.* 203 (2001) 213–231.
- [27] W. J. Ball, S. A. I. Barri, D. Young, EP Patent. 104800, 1984.
- [28] T. Blasc, A. Chica, A. Corma, W. J. Murphy, J. Agúndez-Rodríguez, J. Pérez-Pariente, *J. Catal.* 242 (2006) 153–161.
- [29] S. Gong, N. Chen, S. Nakayama, E. W. Qian, *J. Mol. Catal. A: Chem.* 370 (2013) 14–21.
- [30] S. Gong, A. Shinozaki, E. W. Qian, *Ind. Eng. Chem. Res.* 51 (2012) 13953–13960.
- [31] H. Deldari, *Appl. Catal. A.* 293 (2005) 1–10.
- [32] L. Boda, G. Onyestyák, H. Solt, F. Lónyi, J. Valyon, A. Thernes, *Appl. Catal. A.* 374 (2010) 158–169.
- [33] B. M. Lok, C. A. Messina, R. L. Patton, R. T. Garjek, T. R. Cannan, E. M. Flanigen, USA Patent. 4440871, 1984.
- [34] T. Kabe, E. W. Qian, Y. Hirai, L. Li, A. Ishihara, *J. Catal.* 190 (2000) 191–198.
- [35] E. W. Qian, Q. Zhang, Y. Okoshi, A. Ishihara, T. Kabe, *J. Chem. Soc. Faraday Trans.* 93 (1997) 1821–1826.
- [36] P. Liu, J. Ren, Y. Sun, *Micro. Meso. Mater.* 114 (2008) 365–372.
- [37] J. A. Martens, P. J. Grobet, P. A. Jacobs, *J. Catal.* 126 (1990) 299–305.

- [38] X. Ren, N. Li, J. Cao, Z. Wang, S. Liu, S. Xiang, *Appl. Catal. A*. 298 (2006) 144–151.
- [39] B. M. Lock, C. D. Messina, R. L. Patton, R. T. Gajek, T. R. Cannan, E. M. Flanigen, *J. Am. Chem. Soc.* 106 (1984) 6092–6093.
- [40] Y. Fan, D. Lei, G. Shi, X. Bao, *Catal. Today*. 114 (2006) 388.
- [41] X. Zhang, J. Wang, J. Zhong, A. Liu, J. Gao, *Micro. Meso. Mater.*, 108 (2008) 13-21.
- [42] A. Corma, A. Martinez, S. Pergher, S. Peratello, C. Perego, G. Bellusi, *Appl. Catal. A*. 152 (1997) 107.
- [43] S. Zhang, S. Chen, P. Dong, G. Yuan, K. Xu, *Appl. Catal. A*. 332 (2007) 46–55.
- [44] M. B. Fernández, G. M. Tonetto, G. Crapiste, D. E. Damiani, *Int. J. Chem. React. Eng.* 5 (2007) A10.
- [45] I. Lukić, J. Krstić, D. Jovanović, D. Skala, *Bioresour. Technol.* 100 (2009) 4690–4696.
- [46] C. Baerlocher, L. B. McCusker, D. H. Olson, *Atlas of zeolite framework types*, sixth revised edition, Elsevier, 2007.

**Figure captions**

**Table 1** Physical properties and chemical composition of Jatropha oil.

**Table 2** Physicochemical properties of calcined SAPO-11 samples.

**Table 3** Acidity of calcined SAPO-11 samples.

**Table 4** Gaussian simulation results for the  $^{29}\text{Si}$  NMR MAS spectra of SAPO-11 samples.

**Table 5** Physicochemical properties of Pt/SAPO-11 catalysts.

**Table 6** Conversion of triglycerides and the yields of various products over Pt/SAPO-11 catalysts with varied Si/Al ratios.

**Table 7** Yields of various products over Pt/SAPO-11 catalysts with varied Pt loading.

**Table 8** Results of methyl oleate hydroconversion over Catalyst C at various temperatures.

**Fig. 1.** XRD profiles of calcined SAPO-11 samples.

**Fig. 2.** NH<sub>3</sub>-TPD profiles of calcined SAPO-11 samples. Experimental (—) and simulated (—) spectra using the peak constituents (—). (Peak 1, Low temperature peak; Peak 2, High temperature peak)

**Fig. 3.** <sup>29</sup>Si MAS NMR spectra of calcined SAPO-11 samples. Experimental (—) and simulated (—) spectra using the peak constituents (—). [Peak 1, Si(4Si 1); Peak 2, Si(1Al, 3Si); Peak 3, Si(2Al, 2Si); Peak 4, Si(3Al, Si); Peak 5, Si(4Al)]

**Fig. 4.** Effect of the Si/Al ratio on the yields of various fractions of the liquid hydrocarbon products: (■) C<sub>5-14</sub>, (●) C<sub>15-18</sub>, (▲) C<sub>18+</sub>.

**Fig. 5.** Effect of the Si/Al ratio on the yields of *iso*-C<sub>15-18</sub> hydrocarbon products.

**Fig. 6.** Effect of Pt loading and LHSV on the yields of various fractions: (a) C<sub>15-18</sub>, (b) C<sub>5-14</sub>, (c) C<sub>18+</sub> over (■) Catalyst C, (●) Catalyst E, (▲) Catalyst F.

**Fig. 7.** Effect of Pt loading and LHSV on the ratios of *iso*-C<sub>15-18</sub>/*n*-C<sub>15-18</sub>: (■) Catalyst C, (●) Catalyst E, (▲) Catalyst F.

**Fig. 8.** Yield of methyl stearate (*n*-C<sub>17</sub>H<sub>35</sub>COOCH<sub>3</sub>), octadecanol (*n*-C<sub>18</sub>H<sub>37</sub>OH), heptadecanol (*n*-C<sub>17</sub>H<sub>35</sub>OH), stearic acid (*n*-C<sub>17</sub>H<sub>35</sub>COOH), and octadecyl stearate (*n*-C<sub>17</sub>H<sub>35</sub>COO C<sub>18</sub>H<sub>37</sub>) at different temperatures.

**Fig. 9.** Experimental and theoretical yields of the various gaseous products at different temperatures.

**Scheme 1.** Proposed mechanisms for hydroconversion of methyl oleate over Pt/SAPO-11 catalyst ( $R^-$ ,  $C_{17}H_{33}$ ; R:  $C_{17}H_{35}$ ).

**Scheme 2.** Proposed mechanisms for hydroconversion of Jatropha oil over Pt/SAPO-11 catalyst. ( $R^-$ :  $C_{15}H_{29}$ ,  $C_{17}H_{33}$ , R:  $C_{15}H_{31}$ ,  $C_{17}H_{35}$ ).

Accepted Manuscript

**Table 1**

Physical properties and chemical composition of Jatropha oil.

|                                 | Value |
|---------------------------------|-------|
| Physical properties             |       |
| density (g/cm <sup>3</sup> )    | 0.91  |
| dynamic viscosity (mPa·s/25 °C) | 25.32 |
| acid value (mg KOH/g)           | 7.86  |
| cloud point (°C)                | -4    |
| cetane index                    | 45    |
| Fatty acid composition, C %     |       |
| palmitoleic acid (C16:1)        | 0.93  |
| palmitic acid (C16:0)           | 13.62 |
| linoleic acid (C18:2)           | 36.21 |
| oleic acid (C18:1)              | 43.39 |
| stearic acid (C18:0)            | 5.85  |
| Element analysis                |       |
| C (wt %)                        | 78.2  |
| H (wt %)                        | 12.4  |
| O (wt %)                        | 9.5   |
| S (ppm)                         | 4     |

**Table 2**

Physicochemical properties of calcined SAPO-11 samples.

| Supports     | $S_{\text{BET}}^{\text{a}}$<br>(m <sup>2</sup> /g) | $V_{\text{total}}^{\text{a}}$<br>(cm <sup>3</sup> /g) | $d_{\text{avg}}^{\text{a}}$<br>(nm) | Chemical<br>composition <sup>b</sup>                                     | Relative<br>crystallinity (%) |
|--------------|--|---|-------------------------------------|--|-------------------------------|
| SAPO-11(0.1) | 194  | 0.185   | 3.6                                 | (Al <sub>0.49</sub> P <sub>0.47</sub> Si <sub>0.04</sub> )O <sub>2</sub> | 100                           |
| SAPO-11(0.2) | 190  | 0.151   | 3.2                                 | (Al <sub>0.48</sub> P <sub>0.43</sub> Si <sub>0.09</sub> )O <sub>2</sub> | 98.5                          |
| SAPO-11(0.4) | 172  | 0.147   | 3.4                                 | (Al <sub>0.45</sub> P <sub>0.39</sub> Si <sub>0.16</sub> )O <sub>2</sub> | 76.3                          |
| SAPO-11(0.8) | 129  | 0.133   | 4.7                                 | (Al <sub>0.40</sub> P <sub>0.33</sub> Si <sub>0.27</sub> )O <sub>2</sub> | 57.7                          |

<sup>a</sup> Specific surface area, pore volume and average pore diameter were calculated using the BET method.<sup>b</sup> Chemical composition determined by XRF.<sup>c</sup> Relative crystallinity determined by XRD.

**Table 3**

Acidity of calcined SAPO-11 samples.

| Samples      | Weak                  |                               | Medium                |                               | Total acidity ( $\mu\text{mol/g}$ ) |
|--------------|-----------------------|-------------------------------|-----------------------|-------------------------------|-------------------------------------|
|              | T/ $^{\circ}\text{C}$ | acidity ( $\mu\text{mol/g}$ ) | T/ $^{\circ}\text{C}$ | acidity ( $\mu\text{mol/g}$ ) |                                     |
| SAPO-11(0.1) | 249                   | 248.4                         | 334                   | 223.2                         | 471.6                               |
| SAPO-11(0.2) | 255                   | 297.0                         | 352                   | 300.6                         | 597.6                               |
| SAPO-11(0.4) | 254                   | 268.2                         | 348                   | 389.7                         | 657.9                               |
| SAPO-11(0.8) | 252                   | 250.2                         | 346                   | 396.9                         | 646.1                               |

**Table 4**Gaussian simulation results for the  $^{29}\text{Si}$  NMR MAS spectra of SAPO-11 samples.

| Samples      | Selectivity of various environmental Si (%) |                          |                          |                        |                    |
|--------------|---|--------------------------|--------------------------|------------------------|--------------------|
|              | Si(4Si)<br>-112 ppm                         | Si(1Al, 3Si)<br>-107 ppm | Si(2Al, 2Si)<br>-102 ppm | Si(3Al, Si)<br>-97 ppm | Si(4Al)<br>-90 ppm |
| SAPO-11(0.1) | 8.8   | 12.9                     | 18.7                     | 29.3                   | 30.3               |
| SAPO-11(0.2) | 9.6   | 22.7                     | 22.8                     | 20.9                   | 24.0               |
| SAPO-11(0.4) | 16.6  | 19.3                     | 27.1                     | 18.2                   | 18.8               |
| SAPO-11(0.8) | 17.2  | 30.4                     | 25.1                     | 12.7                   | 14.6               |

**Table 5**

Physicochemical properties of Pt/SAPO-11 catalysts.

| Catalysts | Support      | Pt Content (wt.%) | Pt dispersion (%) | $S_{\text{BET}}$ ( $\text{m}^2/\text{g}$ ) |
|-----------|--------------|-------------------|-------------------|--|
| A         | SAPO-11(0.1) | 0.62              | 61                | 159  |
| B         | SAPO-11(0.2) | 0.56              | 59                | 152  |
| C         | SAPO-11(0.4) | 0.58              | 54                | 146  |
| D         | SAPO-11(0.8) | 0.55              | 38                | 95   |
| E         | SAPO-11(0.4) | 1.41              | 44                | 136  |
| F         | SAPO-11(0.4) | 2.78              | 36                | 125  |

**Table 6**

Conversion of triglycerides and the yields of various products over Pt/SAPO-11 catalysts with varied Si/Al ratios.

| Catalyst                        | Catalyst A | Catalyst B | Catalyst C | Catalyst D |
|---------------------------------|------------|------------|------------|------------|
| Conversion of triglycerides (%) | 100.0      | 100.0      | 100.0      | 98.3       |
| Yields based on feedstock (wt%) |            |            |            |            |
| Liquid hydrocarbon              | 83.0       | 82.9       | 82.8       | 84.9       |
| Gas hydrocarbon                 | 5.6        | 5.6        | 5.7        | 5.9        |
| CO + CO <sub>2</sub>            | 1.8        | 0.8        | 1.0        | 2.4        |
| Water                           | 9.8        | 10.3       | 10.2       | 9.5        |

T = 350 °C, LHSV = 1 h<sup>-1</sup>, P = 3 MPa, H<sub>2</sub>/Oil = 1200 ml/ml.

**Table 7**

Yields of the various products over Pt/SAPO-11 catalysts with varied Pt loading.

| Catalyst   | LHSV (h <sup>-1</sup> ) | Conversion of triglycerides (%) | Yields based on feedstock (wt%) |                 |                    |       |
|------------|-------------------------|---------------------------------|---------------------------------|-----------------|--------------------|-------|
|            |                         |                                 | Liquid hydrocarbon              | Gas hydrocarbon | CO+CO <sub>2</sub> | Water |
| Catalyst C | 0.25                    | 100                             | 75.1                            | 9.3             | 1.8                | 9.7   |
|            | 0.5                     | 100                             | 77.2                            | 7.9             | 1.6                | 9.9   |
|            | 1                       | 100                             | 82.8                            | 5.7             | 0.8                | 10.3  |
| Catalyst E | 0.5                     | 100                             | 71.6                            | 10.1            | 2.0                | 9.7   |
|            | 1                       | 100                             | 76.6                            | 8.1             | 1.2                | 10.1  |
|            | 1.5                     | 100                             | 83.2                            | 5.6             | 0.9                | 10.2  |
| Catalyst F | 0.5                     | 100                             | 65.3                            | 13.3            | 2.4                | 9.5   |
|            | 1                       | 100                             | 74.8                            | 9.2             | 1.6                | 9.9   |
|            | 1.5                     | 100                             | 78.5                            | 7.1             | 1.4                | 10.0  |
|            | 2                       | 100                             | 81.2                            | 5.7             | 0.5                | 10.4  |

T = 350 °C, P = 3 MPa, H<sub>2</sub>/Oil = 1200 ml/ml

**Table 8**

Results of methyl oleate hydroconversion over Catalyst C at various temperatures.

| Temperature/°C   | 200   | 225   | 250   | 275   | 300   | 325   |
|--|-------|-------|-------|-------|-------|-------|
| Conversion (%)   | 98.47 | 100   | 100   | 100   | 100   | 100   |
| Deoxygenation rate (%)   | 6.31  | 11.99 | 48.86 | 90.82 | 100   | 100   |
| Yield of gaseous products (C%)   |       |       |       |       |       |       |
| CH <sub>4</sub>  | 0.14  | 1.23  | 4.12  | 7.05  | 7.91  | 7.92  |
| CO   | 0.00  | 0.00  | 0.00  | 0.00  | 0.00  | 0.01  |
| CO <sub>2</sub>  | 0.00  | 0.00  | 0.01  | 0.03  | 0.04  | 0.04  |
| Yield of C <sub>17,18</sub> hydrocarbons (C%)                                |       |       |       |       |       |       |
| <i>n</i> -C <sub>17</sub> H <sub>36</sub>                                    | 0.18  | 2.03  | 17.86 | 37.51 | 25.04 | 19.08 |
| <i>n</i> -C <sub>18</sub> H <sub>38</sub>                                    | 0.43  | 1.85  | 16.18 | 35.80 | 22.91 | 17.79 |
| <i>i</i> -C <sub>17</sub> H <sub>36</sub>                                    | 0.02  | 0.18  | 1.66  | 4.02  | 21.84 | 26.59 |
| <i>i</i> -C <sub>18</sub> H <sub>38</sub>                                    | 0.02  | 0.13  | 1.22  | 3.89  | 20.22 | 25.06 |
| Yield of total oxygenates (C%)   |       |       |       |       |       |       |
| <i>n</i> -C <sub>17</sub> H <sub>35</sub> OH                                 | 0.00  | 1.40  | 1.26  | 0.78  | 0.00  | 0.00  |
| <i>n</i> -C <sub>18</sub> H <sub>37</sub> OH                                 | 0.29  | 2.89  | 2.41  | 0.52  | 0.00  | 0.00  |
| <i>n</i> -C <sub>17</sub> H <sub>35</sub> COOCH <sub>3</sub>                 | 95.91 | 78.73 | 43.94 | 6.56  | 0.00  | 0.00  |
| <i>n</i> -C <sub>17</sub> H <sub>35</sub> COOH                               | 0.46  | 2.56  | 2.19  | 0.32  | 0.00  | 0.00  |
| <i>n</i> -C <sub>17</sub> H <sub>35</sub> COOC <sub>18</sub> H <sub>37</sub> | 1.35  | 7.15  | 6.35  | 3.31  | 0.00  | 0.00  |
| Ratio of C <sub>17</sub> /C <sub>18</sub>                                    | -     | 1.18  | 1.19  | 1.11  | 1.15  | 1.13  |
| Ratio of <i>iso</i> -C <sub>17+18</sub> / <i>n</i> -C <sub>17+18</sub>       | -     | 0.08  | 0.08  | 0.11  | 0.88  | 1.40  |

LHSV = 40h<sup>-1</sup>, P = 3 MPa, H<sub>2</sub>/Oil = 1200 ml/ml.

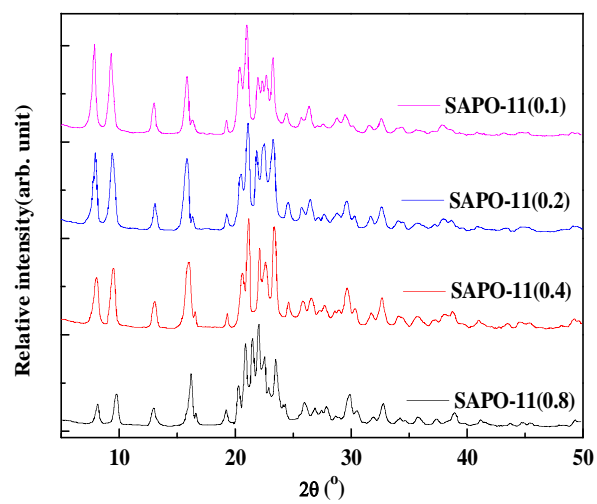


**Fig. 1.** XRD profiles of calcined SAPO-11 samples.

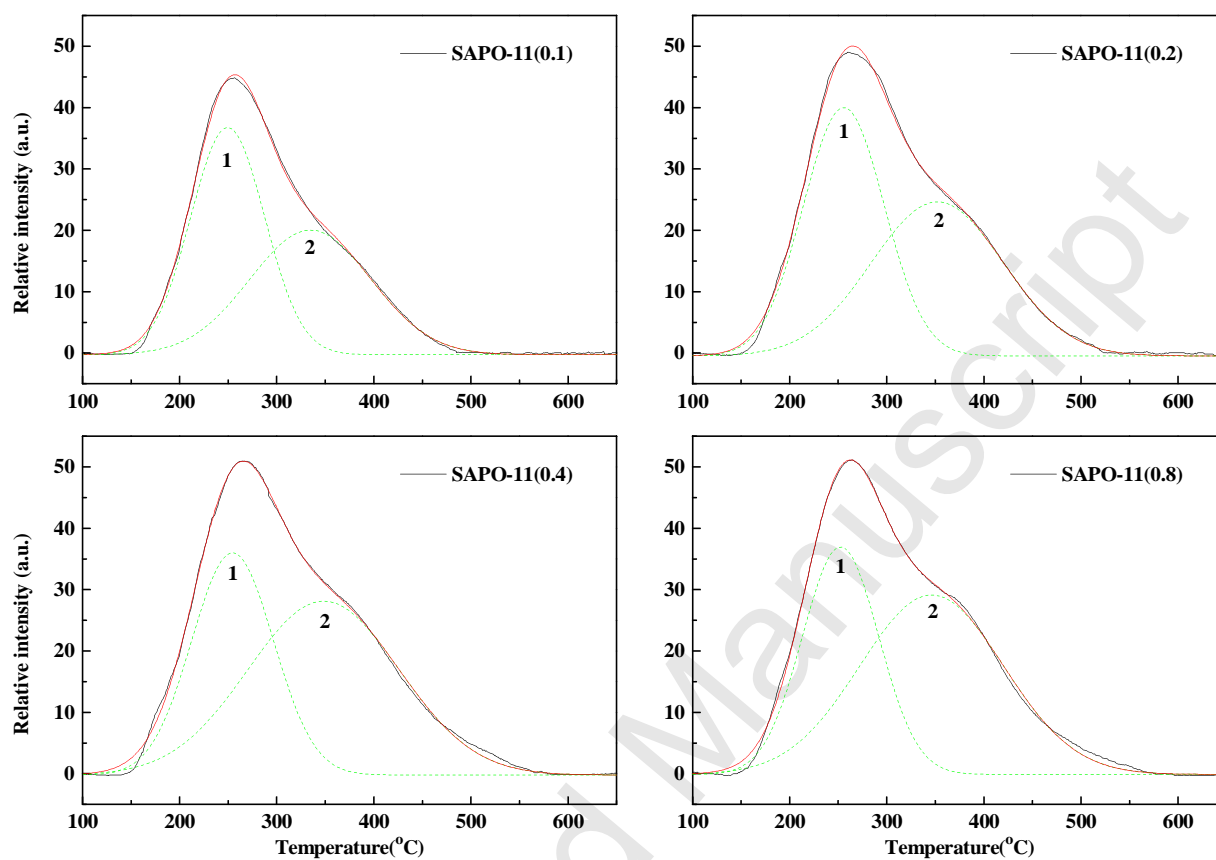


**Fig. 2.** NH<sub>3</sub>-TPD profiles of calcined SAPO-11 samples. Experimental (—) and simulated (—) spectra using the peak constituents (---). (Peak 1, Low temperature peak; Peak 2, High temperature peak)

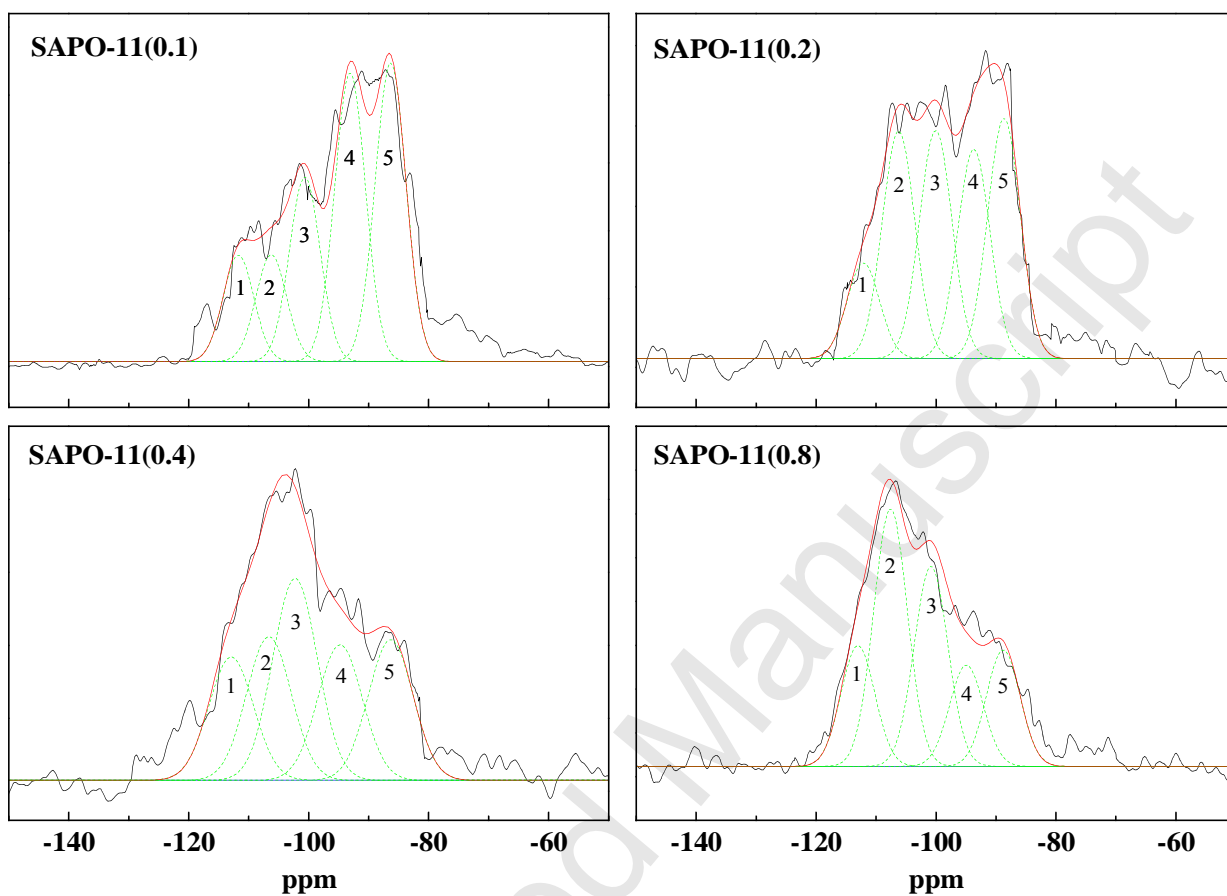


**Fig. 3.**  $^{29}\text{Si}$  MAS NMR spectra of calcined SAPO-11 samples. Experimental (—) and simulated (—) spectra using the peak constituents (---). [Peak 1, Si(4Si 1); Peak 2, Si(1Al, 3Si); Peak 3, Si(2Al, 2Si); Peak 4, Si(3Al, Si); Peak 5, Si(4Al)]

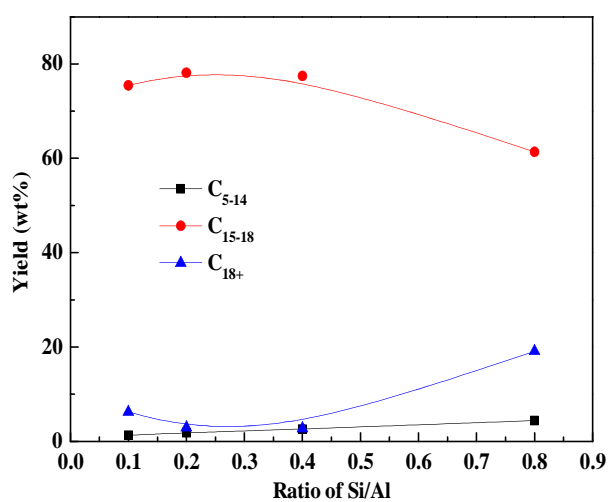


**Fig. 4.** Effect of the Si/Al ratio on the yields of various fractions of the liquid hydrocarbon products: (■) C<sub>5-14</sub>, (●) C<sub>15-18</sub>, (▲) C<sub>18+</sub>.

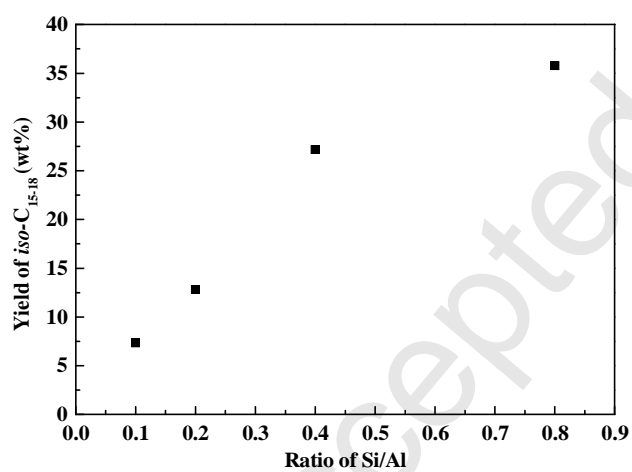


**Fig. 5.** Effect of the Si/Al ratio on the yields of iso-C<sub>15-18</sub> hydrocarbon products.

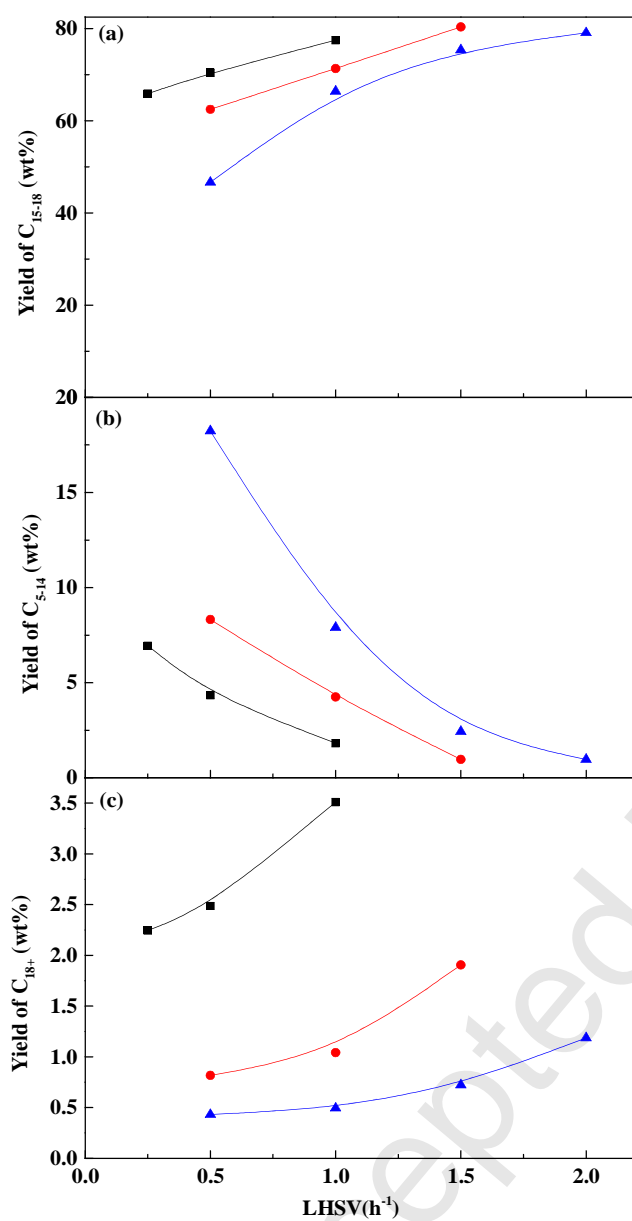


**Fig. 6.** Effect of Pt loading and LHSV on the yields of various fractions: (a) C<sub>15-18</sub>, (b) C<sub>5-14</sub>, (c) C<sub>18+</sub> over (■) Catalyst C, (●) Catalyst E, (▲) Catalyst F.

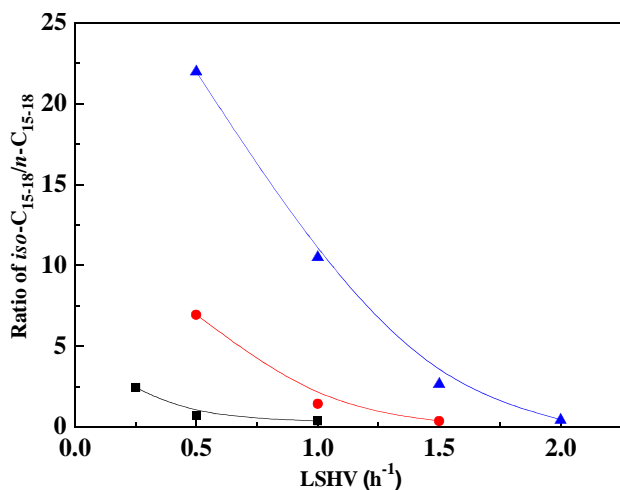


**Fig. 7.** Effect of Pt loading and LHSV on the ratios of *iso*-C<sub>15-18</sub>/*n*-C<sub>15-18</sub>: (■) Catalyst C, (●) Catalyst E, (▲) Catalyst F.

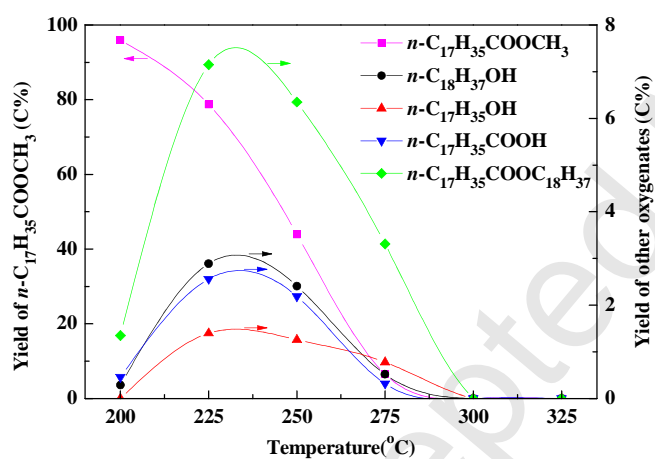


**Fig. 8.** Yield of methyl stearate (*n*-C<sub>17</sub>H<sub>35</sub>COOCH<sub>3</sub>), octadecanol (*n*-C<sub>18</sub>H<sub>37</sub>OH), heptadecanol (*n*-C<sub>17</sub>H<sub>35</sub>OH), stearic acid (*n*-C<sub>17</sub>H<sub>35</sub>COOH), and octadecyl stearate (*n*-C<sub>17</sub>H<sub>35</sub>COO C<sub>18</sub>H<sub>37</sub>) at different temperatures.

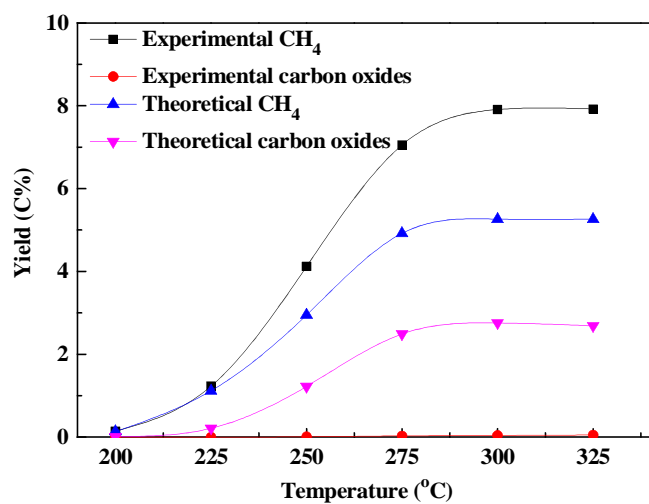


**Fig. 9.** Experimental and theoretical yields of the various gaseous products at different temperatures.



